A&A 447, 441–451 (2006)
DOI: 10.1051/0004-6361:20053204

Astronomy & Astrophysics

NGC 7679: an anomalous, composite Seyfert 1 galaxy whose X-ray luminous AGN vanishes at optical wavelengths⋆

L. M. Buson[1], M. Cappellari[2], E. M. Corsini[3,4], E. V. Held[1], J. Lim[5], and A. Pizzella[3]

[1] INAF Osservatorio Astronomico di Padova, vicolo dell'Osservatorio 5, 35122 Padova, Italy
e-mail: buson@pd.astro.it
[2] Leiden Observatory, Postbus 9513, 2300 RA Leiden, The Netherlands
[3] Dipartimento di Astronomia, Università di Padova, vicolo dell'Osservatorio 2, 35122 Padova, Italy
[4] Scuola Galileiana di Studi Superiori, via VIII Febbraio 2, 35122 Padova, Italy
[5] Institute of Astronomy and Astrophysics, Academia Sinica, PO Box 23-141, Taipei 106, Taiwan

Received 6 April 2005 / Accepted 24 September 2005

ABSTRACT

Morphological disturbances and gas kinematics of the SB0 galaxy NGC 7679 = Arp 216 are investigated to understand the history of this highly composite object, where AGN and starburst signatures dominate in the X-ray and optical/IR regime, respectively. Perturbations of the ionized gas velocity field appear quite mild within 15″ (∼5 kpc) of the center, so it can be straightforwardly modeled as a circularly rotating disk. Outside that radius, significant disturbances are seen. In particular, the eastern distorted arm as well as the huge neutral hydrogen bridge connecting NGC 7679 to the nearby Seyfert spiral NGC 7682 unambiguously represent the vestige of a close encounter of the two objects ∼500 Myr ago. The relationship of such a past event with the much more recent, centrally located starburst (not older than 20 Myr) cannot be easily established. Together, the classification of NGC 7679 is less extreme than that proposed in the past, being simply a (disturbed) galaxy where starburst and AGN activity coexist with a starburst dominating the bolometric luminosity.

Key words. galaxies: individual: NGC 7679 – galaxies: kinematics and dynamics – galaxies: starburst – galaxies: interaction – galaxies: Seyfert

1. Introduction

The barred galaxy we discuss in detail here, NGC 7679, has all the necessary "qualifications" to be regarded as a rare member of a class of composite (AGN/starburst) systems whose X-ray bright Seyfert nucleus becomes unexpectedly weak at optical wavelengths. Alhough a few objects of this kind are known since observations with the Einstein spacecraft (e.g. Elvis et al. 1981) and are currently identified in Chandra deep fields (e.g. Fiore et al. 2000), NGC 7679 could represent a low-redshift example of such peculiar objects showing anomalous absorption processes, i.e. hosting dusty ionized absorbers capable of selectively obscuring the AGN optical emission, while leaving its X-ray emission almost unabsorbed (cf. Della Ceca et al. 2001).

Other well-known obscured Type-2 AGNs, NGC 4945 and NGC 6240 (see Matt 2001, and references therein) are reminiscent of the phenomenology showed by NGC 7679 (e.g. the full emergence of the powerful AGN emission only in the X-ray waveband). NGC 7679, however, is so peculiar as to challenge the standard AGN Unification Scheme since – presumably – its absorption processes can work quite differently, so as to leave its X-ray emission *totally* unabsorbed, while producing a limited amount of absorption of the AGN in the optical (or, alternatively, hosting an optically underluminous Seyfert 1 nucleus; cf. Della Ceca et al. 2001).

Simply classified as SB0p in the Third Reference Catalogue of Bright Galaxies (RC3; de Vaucouleurs et al. 1991), NGC 7679 appears unmistakably disturbed, so as to have been included in the Arp's catalog of peculiar galaxies (Arp 1966). In particular, its asymmetric morphology points toward a barred Seyfert companion (NGC 7682), lying only ∼4′.5 North-East of it. The recession velocity of NGC 7682 ($V_{3\,\mathrm{K}} = 4762 \pm 19$ km s^{-1}) is virtually identical to that of NGC 7679 ($V_{3\,\mathrm{K}} = 4778 \pm 13$ km s^{-1}), once both are referred to the 3 K background on the basis of their RC3 redshift and cosmological parameters $H_0 = 75$ km s^{-1} Mpc^{-1} and $q_0 = 0$. We adopt here the distance of NGC 7679 of 63.9 Mpc; at such a distance 1′ is equivalent to ∼19 kpc and the projected distance of the two galaxies becomes 83.7 kpc.

⋆ Based on observations obtained with the New Technology Telescope at the European Southern Observatory (ESO 63.N-0024B) in La Silla (Chile), with the Multiple Mirror Telescope – a joint facility of the Smithsonian Institution and the University of Arizona (USA) – and with the 1.82-m telescope at the Mount Ekar Observatory in Asiago (Italy).

This object received only sporadic attention in the literature in the past two decades. The optical spectroscopic survey of Dahari (1985) includes NGC 7679 in the transition class of H II/LINER objects. A pioneering investigation of its ionized gas velocity field was performed by Durret & Warin (1990), in the context of their study of extended nebulosities surrounding AGNs. The first deep insight into its starburst nature was provided by the narrow-band Hα imaging survey of Pogge & Eskridge (1993) who reveal the presence of a roundish, nuclear star-forming complex, consisting of bright clumps. An estimate of the relative contribution of its very young population component (a few Myr old) has been derived only recently by Gu et al. (2001), by means of spectral synthesis techniques.

As far the galaxy's activity is concerned, an optical classification as a *Seyfert 2* nucleus is given by Veilleux et al. (1995) and such a classification is kept in the 10th edition of the Catalogue of Quasars and Active Nuclei (Veron & Veron 2001). A proper description of the composite (Seyfert+H II) nature of the object, again on the basis of optical data alone, can be found in Kewley et al. (2001). The full power of the AGN at the center of NGC 7679 was shown in the X-ray domain by means of both BeppoSAX and ASCA observations which reveal a bright and variable central source (Della Ceca et al. 2001). Unlike previous classifications, these authors conclude that the only kind of AGN consistent with its X-ray properties is a Seyfert 1 nucleus.

In the following we make use of narrow-band imaging, optical and UV spectroscopy, as well as of radio observations to characterize the role of the plausible close encounter of the two galaxies, to quantify the central current star formation episode in NGC 7679 and – speculatively – to investigate whether the onset of activity in both nuclei is related to a such past event. In particular, (i) we show in detail the pattern of star-forming regions close to NGC 7679 nucleus; (ii) we compare the inner ionized-gas velocity field of the galaxy with the extended velocity field of the neutral hydrogen component; (iii) we constrain both age and current star formation rate of the current starburst and, finally; (iv) try to place this rich phenomenology in the context of the discussed AGN-starburst connection.

2. Observations and data reduction

2.1. Optical imaging

Narrow-band imaging of NGC 7679 was obtained under good seeing conditions (0.8″ *FWHM*) on September 28, 1999 with the European Southern Observatory (ESO) Multi-mode Instrument (EMMI) of the 3.58 m New Technology Telescope (NTT). The detector was the Tektronix TK2048 CCD mounted on the EMMI Red Channel, giving an effective pixel size of 0.27″ with a 9.′1 × 8.′6 field of view. The on-band and off-band Hα filters were ESO #598 and #596, centered at λ_c = 6685 Å and λ_c = 6568 Å and having a nominal *FWHM* of $\Delta\lambda$ = 67 Å and $\Delta\lambda$ = 73 Å, respectively. An exposure time of 600 s was adopted for both science frames, while a shorter (200 s) exposure of the star Feige 110 was obtained through the on-band filter for calibration purposes.

Using standard MIDAS[1] routines the images were bias subtracted, corrected for flat field using sky flats and cleaned for cosmic rays. The sky background level was removed as a constant value estimated in regions free of sources in the images. The two consecutive NGC 7679 images obtained through the off-band/on-band filters, respectively, were shifted and aligned using common field stars. The point spread function (PSF) of the Hα image shows a slight North-West/South-East elongation not seen in the adjacent continuum image. After performing several convolution tests to match the two PSFs, we subtracted directly the scaled off-band continuum from the on-band image in order to keep as much as possible the fine detail of the emission-line features allowed by the good seeing conditions. The best scaling parameter turned out to be very close to unity, as expected from the relative efficiencies and bandwidths for the on-band and off-band filter. A fine tuning of this parameter, obtained by imposing that the resulting continuum-subtracted image does not show spurious negative areas, did confirm that the best choice was to avoid any kind of re-scaling before subtraction.

Flux calibration was derived by means of the observation of the star Feige 110. Under the assumption that the sensitivity and the absolute flux for Feige 110 are constant across the on-band filter, following Sparks et al. (1993) one can estimate the sensitivity function (in erg cm^{-2} count^{-1}) at the redshifted Hα on the basis of the measured star count rate (in count s^{-1}) and equivalent width of the filter. This parameter, in turn, provides the needed conversion to derive the total emission-line flux $F_{\mathrm{H}\alpha+[\mathrm{NII}]}$ from the observed count rate for the chosen galaxy region. The derived flux was later corrected for atmospheric extinction.

2.2. Optical spectroscopy

The long-slit spectroscopic observations of NGC 7679 were carried out at the European Southern Observatory in La Silla (Chile) with the ESO 1.52-m telescope (runs 1 and 4−5), at the Mt. Ekar Observatory in Asiago (Italy) with the 1.82-m telescope (runs 2 and 3), and at the Multiple Mirror Telescope Observatory in Arizona with the Multiple Mirror Telescope (MMT, run 6). The details about the instrumental setup of each observing run are given below in Table 1.

Different medium-resolution spectra (runs 1, 2, 3, 5, and 6) were taken along several axes after centering the galaxy nucleus on the slit using the guiding camera. Two low-resolution spectra (run 4) were taken with the long slit crossing the nucleus along the North-South direction. An overall picture of the velocity field sampling assured by our set of medium-resolution spectra is shown in Fig. 1. A lamp spectrum was taken before and/or after each science exposure for wavelength calibration purposes.

Basic data reduction was performed as in Corsini et al. (1999). Using standard `ESO-MIDAS` routines, all the spectra were bias subtracted, flat-field corrected by quartz lamp and twilight exposures, cleaned of cosmic rays, and wavelength

[1] MIDAS is developed and maintained by the European Southern Observatory.

Table 1. Instrumental setup and log of spectroscopic observations.

Parameter	Run 1	Run 2	Run 3	Run 4	Run 5	Run 6
Date	21 Nov. 1987	06 Sep. 1992	25-26 Sep. 1994	26 Sep. 1998	10 Sep. 1999	2 Nov. 2002
Telescope	1.52-m ESO	1.82-m Ekar	1.82-m Ekar	1.52-m ESO	1.52-m ESO	MMT
Spectrograph	B&C	B&C	B&C	B&C	B&C	Blue Channel
Grating[a] (gr mm^{-1})	#12 1200	1200	1200	#25 400	#33 1200	1200
Detector	#13 RCA	Thomson TH7882	Thomson TH7882	#39 Loral-Lesser	#39 Loral-Lesser	#22 Loral
Detector size (pixels)	1024 × 640	580 × 388	580 × 388	1024 × 1024	1024 × 1024	3072 × 1024
Pixel size (μm^2)	15 × 15	23 × 23	23 × 23	15 × 15	15 × 15	15 × 15
Pixel binning	1 × 1	1 × 1	1 × 1	1 × 1	1 × 1	1 × 1
Scale ($''$ pixel^{-1})	0.68	1.23	1.23	0.82	0.82	0.30
Dispersion (Å pixel^{-1})	0.864	1.025	1.025	2.81	0.985	0.49
Slit width ($''$)	1.3	3.7	5.3	2.0	2.2	1.5
Slit length ($'$)	4.5	5.8	5.8	4.1	4.1	2.5
Spectral range (Å)	5840–6730	6260–6820	6300–6880	3350–9300	4860–6860	4460–5950
Comparison lamp	He–Ar	He–Ar	He–Ar	He–Ar	He–Ar	He–Ar–Ne
Instr. *FWHM* (Å)	1.64 ± 0.12	1.73 ± 0.04	2.50 ± 0.03	9.65 ± 0.38	2.99 ± 0.01	2.02 ± 0.02
Instr. σ[b] (km s^{-1})	32	34	49	187	58	53
Seeing *FWHM* ($''$)	1.0–1.5	1.5–2.0	1.5–2.5	0.8–1.0	2.0–3.0	1.8–2.2
Observed PA (°)	3, 93	63, 78, 93, 108, 123	28, 48, 138, 158	0	87	87
Exposure time (s)	3600	2400	3600	2 × 900	2 × 3600	2700

[a] The grating has been used at the first order.
[b] The instrumental velocity dispersion as measured at Hα.

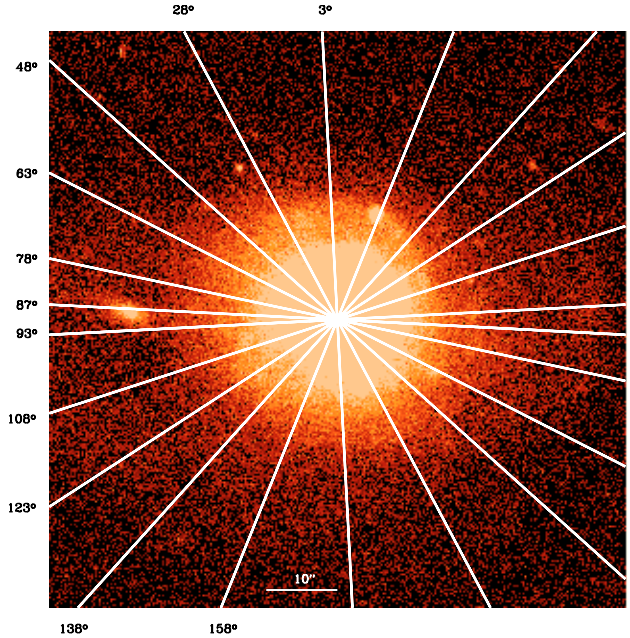

Fig. 1. The angular coverage of our medium-resolution long-slit spectra of NGC 7679. The lines mark the nominal position of the slits.

calibrated. The flat-field correction was performed by means of both quartz lamp and twilight sky spectra in order to correct for pixel-to-pixel sensitivity variations and large-scale illumination patterns due to slit vignetting. Cosmic rays were identified by comparing the photon counts in each pixel with the local mean and standard deviation and they were eliminated by interpolation. Residual cosmic rays were eliminated by manually editing the spectra. We checked that the wavelength rebinning was done properly by referring to the brightest night-sky emission lines in the observed spectral ranges. The resulting accuracy in the wavelength calibration is typically 5 km s^{-1}.

For each observing run the instrumental resolution was derived in the spectral region of the Hα emission line as the mean of Gaussian *FWHM*s measured for a number of unblended arc-lamp lines of a wavelength-calibrated comparison spectrum. The mean *FWHM* of the arc-lamp lines and the corresponding resolution at Hα are given in Table 1. After the calibration, all the spectra were corrected for CCD misalignment. The contribution of the sky was determined from the outermost ∼20$''$ at the two edges of the resulting frames where the galaxy light was negligible, and then subtracted. In runs 4 and 5 the two spectra obtained at PA = 87° were coadded using the center of the stellar-continuum radial profile as reference. In run 4 we observed some spectrophotometric standard stars to allow the flux calibration of the low-resolution spectra.

2.3. Ultraviolet spectroscopy

The occurrence of a powerful star formation event in NGC 7679 is made clear by the availability in the International Ultraviolet Explorer (IUE) archives of a long-exposure (∼7 h), large aperture (∼10$''$ × 20$''$) SWP spectrum covering the wavelength range 1200−1900 Å. Unlike the majority of IUE spectra of nearby galaxies, the relatively high redshift of this object allows the Lyα emission of its disk to appear fully detached from the contaminating geocoronal Lyα. Such an intrinsic line is indeed quite strong and extended (∼12$''$) along the spatial direction (at PA = 134°).

The IUE spectrum has been re-extracted by means of our own MIDAS routines. We started from the so-called NEWSIPS spatially-resolved, low-resolution image (SILO), obtained from the archive of the Italian National Host of INES (IUE Newly Extracted Spectra) distribution system. The properly fluxed, redshift and galactic reddening corrected UV spectrum is presented and discussed below. The adopted foreground galactic extinction was $E(B-V) = 0.06$ from Burstein & Heiles (1984).

2.4. Radio observations

The presence of an extended H I halo around NGC 7679 *and* its companion galaxy NGC 7682 has been pointed out by observations carried out at Arecibo Observatory since 1986 (Duprie & Schneider 1996). They derive for either galaxy a neutral gas mass $M_{\rm HI} \sim 5 \times 10^9\ M_\odot$. A subsequent work of Kandalyan (2003), taking into account radio CO line observations, indicates that NGC 7679 possesses a comparable amount of molecular hydrogen ($M_{\rm H2} \sim 6 \times 10^9\ M_\odot$).

Our recent observations of NGC 7679 and its neighbor NGC 7682 in the 21-cm line of H I were obtained on July 28 and August 20, 2000 using the D configuration (i.e. the best-suited to detect faint extended emission) of the NRAO Very Large Array (VLA)[2]. Both galaxies, with an angular separation of ~7.′5, easily fit into the field of view of the VLA, which has half-power beamwidth at 21 cm of ~1′. The VLA correlator was configured so as to provide a velocity resolution of ~21 km s^{-1}. The total on-source time was ~2.0 h. The data were calibrated, continuum subtracted and mapped in the standard fashion using the Astronomical Image Processing System (AIPS).

3. Results

3.1. The optical morphology

The NGC 7679 continuum, the overall continuum-subtracted pure emission image, and innermost spiral-like circumnuclear emitting region are shown in Fig. 2.

The distribution of the "pure" Hα+[N II] emission consists mainly of a roundish component hiding a brighter, very central spiral-like structure. Thanks to the higher NTT/EMMI dynamical range and resolution, such an image represents an evident improvement over the emission-line image recorded by Pogge & Eskridge (1993).

In particular the circumnuclear complex morphology indicates that the starburst activity goes down to the very central regions. Moreover, both its appearance and absolute size are reminiscent of the circumnuclear starburst in NGC 5248 that is interpreted as induced by a stellar bar in the very central region as recently discussed by Jogee et al. (2002).

[2] The National Radio Astronomy Observatory is operated by the Associated Universities, Inc., under cooperative agreement with the National Science Foundation.

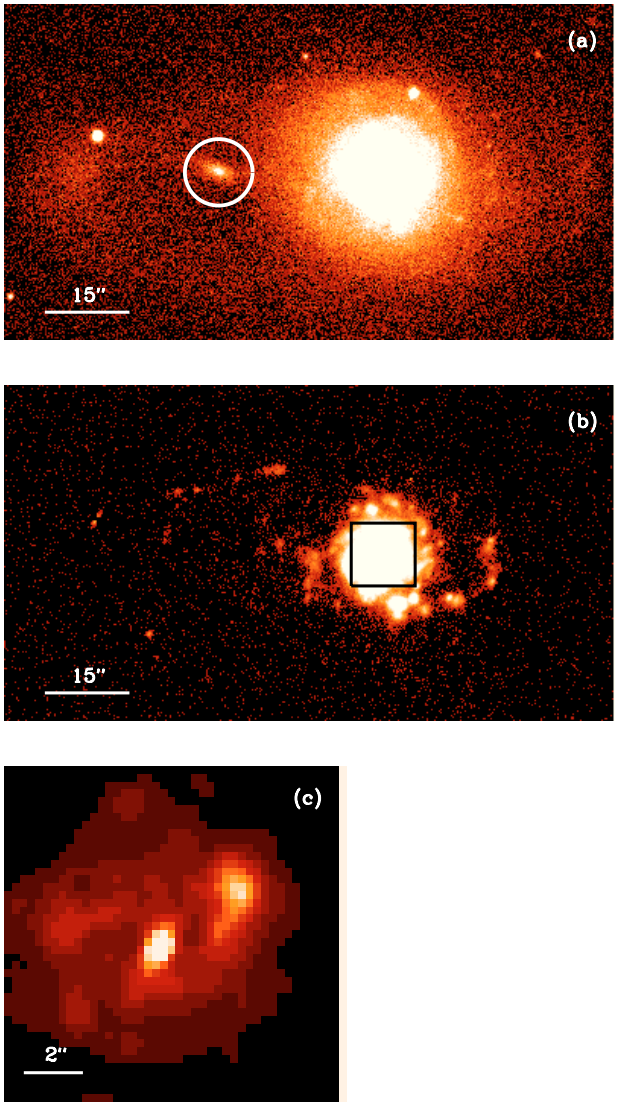

Fig. 2. a) Narrow-band continuum image of NGC 7679 and its surrounding distorted arm. North is up and East on the left. The circled object is a background galaxy not involved in the outer tidal distortion of NGC 7679 (see discussion below). **b)** Pure Hα+[N II] image of the same field showing individual bright knots and loose gaseous debris; the squared inset is zoomed in panel **c)** in order to show the circumnuclear emitting region.

3.2. The ionized-gas velocity field

The rotation curves and the velocity dispersion profiles we measured along the observed axes of NGC 7679 are shown in Fig. 3.

The line-of-sight velocities and velocity dispersions of the ionized-gas component were measured by means of the `MIDAS` package `ALICE`. At each radius, we measured the Hα, [N II] $\lambda\lambda$6548, 6583 and [S II] $\lambda\lambda$6716, 6731 emission lines where they were clearly detected. The position, the *FWHM*, and the uncalibrated flux of each emission line were determined by interactively fitting one Gaussian to each line plus a polynomial to its local continuum. The central wavelength of the fitting Gaussian was converted into velocity in the optical convention and the standard heliocentric correction was applied.

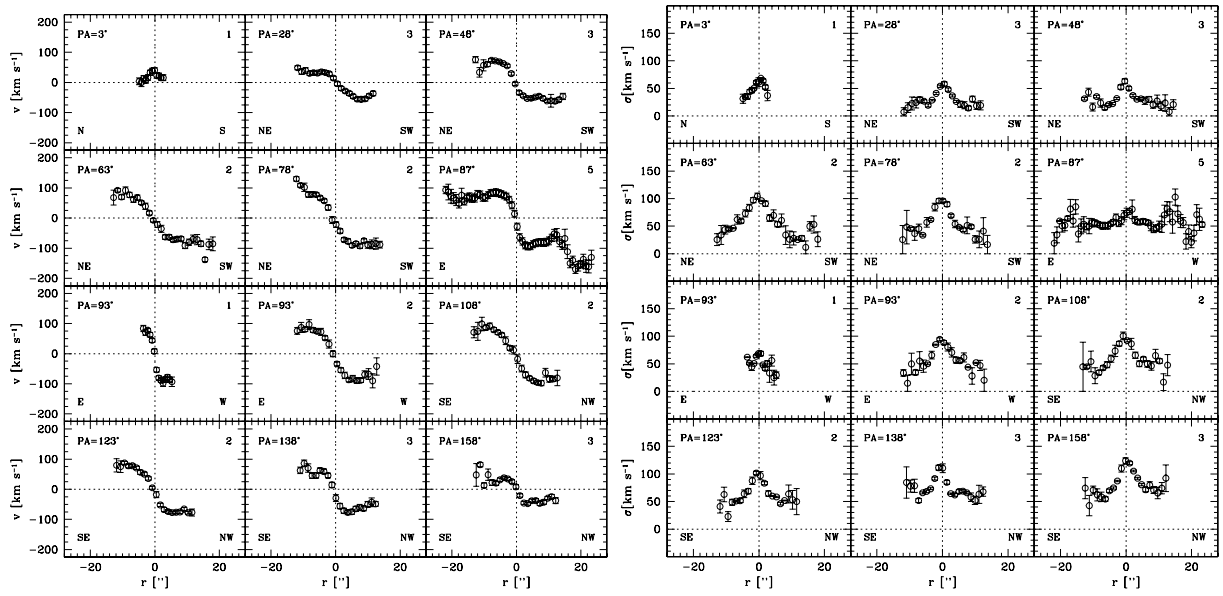

Fig. 3. Ionized-gas rotation velocity curves (*left panels*) and velocity dispersion profiles (*right panels*) measured along the observed axes of NGC 7679. Plotted velocities are subtracted by systemic velocity and not corrected for galaxy inclination. Each subframe contains both the corresponding PA (*upper left*) as well as the observing run number (*upper right*; see Table 1).

The heliocentric systemic velocity ($V_\odot = 5165 \pm 5$ km s^{-1}) was derived from the center of symmetry of the rotation curve along the galaxy major axis. It corresponds to $V_{3\,\mathrm{K}} = 4796$ km s^{-1} after applying the 3 K background correction following Fixsen et al. (1996). Note that the latter value derived by us is consistent, within the error, with the previous, analogously corrected RC3 velocity given in the introduction. The Gaussian *FWHM* was corrected for the instrumental *FWHM*, and then converted into the velocity dispersion. In the regions where the intensity of the emission lines was low, we binned adjacent spectral rows in order to improve the signal-to-noise ratio of the lines.

The velocity profiles presented in Fig. 3 display a high degree of symmetry within the central regions, suggesting that they may be well represented by a simple disk geometry. To determine whether a regular disk rotation can explain the observed gas kinematics we used the kinemetry software by Krajnović et al. (2005) to construct the best fitting non-parametric disk model of the gas kinematics within the innermost 15″ from the galaxy nucleus. The idea behind our procedure is that for a disk that is observed at an inclination i, an ellipse of axial ratio $q = \cos i$ and the same position angle as the disk, will sample equal radii in the disk plane. Moreover, if the motion is purely circular, the observed velocity along that ellipse will be described by a cosine law. Our procedure consists of iteratively changing the inclination until these two conditions are satisfied. In more detail we performed the following steps:

1. We assumed an observed inclination i and a projected position angle (PA) for the gas disk;
2. we sampled the observed velocity V along a set of ellipses, regularly spaced in the semimajor axis, with constant $q = \cos i$ and PA as defined above, using linear interpolation when needed to estimate the velocity;
3. along each ellipse of semimajor axis R we least-squares fitted the velocity with the formula $V_\mathrm{d}(R,\theta) = V_0(R)\cos\theta$, which describes the line-of-sight velocity along the disk where the circular velocity is $V_\mathrm{c}(R) = V_0(R)/\sin i$. Here θ is the eccentric anomaly, measured from the projected major axis of the ellipse;
4. we computed the model velocity $V_\mathrm{d}(x,y)$ at the observed N coordinates (x,y) on the sky using linear interpolation;
5. we determined the agreement between the observed velocity field and the disk model as $\chi^2 = \sum_{j=1}^{N}[(V_{\mathrm{d},j} - V_j)/\Delta V]^2$, where ΔV are the measurements errors;
6. we iterated the points 1–5 for a regular grid of q and PA values. We finally selected the best fitting values and the corresponding errors from the contours of $\chi^2(q, \mathrm{PA})$.

The result of the above procedure provided the best fitting disk parameter $q = \cos(i) = 0.90 \pm 0.05$ and PA $= 93 \pm 3$ (3σ errors). The interpolated data and the ellipses along which the velocity was sampled are presented in the top panel of Fig. 4,

While the best fitting disk model is shown in the middle panel. The residuals between the data and the best fitting model are displayed in the bottom panel. It is apparent that the observation can be remarkably well described by the adopted simple thin disk approximation. The best fitting $\chi^2 \sim 2$ also indicates that the gas kinematics in the central is marginally consistent with a pure nearly face-on ($i \approx 26°$) disk model. No obvious regular features are apparent in the residual map, suggesting that the difference of the χ^2 from unity is due only to residual systematics in the different data sets. Unfortunately the near face-on geometry of the observed disk, and the small spatial extension of the data, is unfavorable for a detailed mass modeling of this galaxy, due to large uncertainties in the mass deprojection and inclination effects. We will not explore this further in this paper.

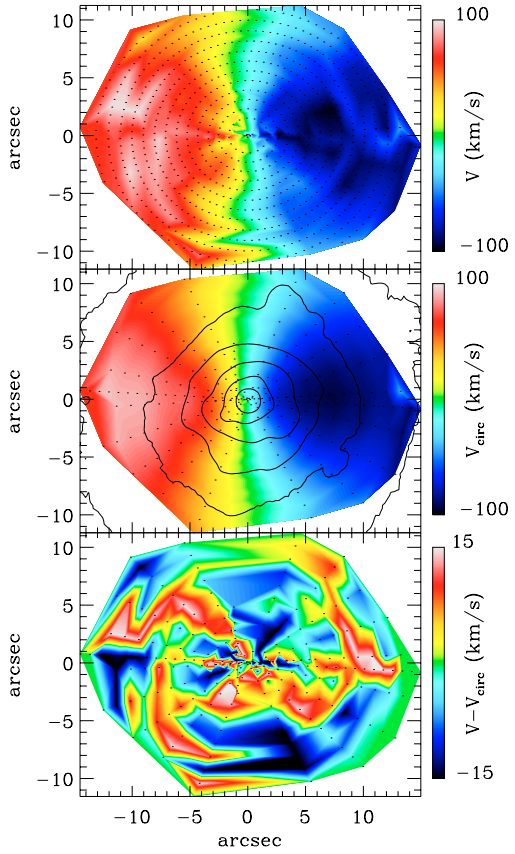

Fig. 4. Interpolated velocity field and sampling ellipses (*top panel*), best fitting velocity field for a disk model (*middle panel*), and residuals between interpolated and best fitting velocity field (*bottom panel*) for the ionized gas component of NGC 7679 within 15″ from the center.

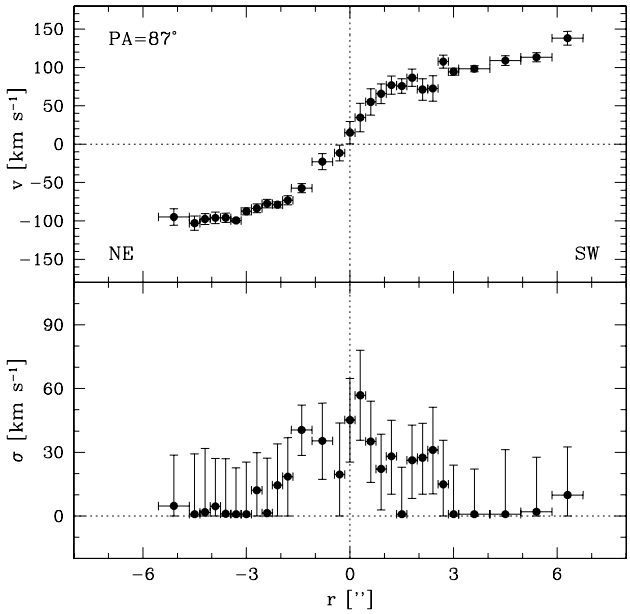

Fig. 5. The derived gaseous rotation curve and velocity dispersion profile of the background object projected on the outskirts of NGC 7679. The scale is ∼2 kpc arcsec^{-1}.

3.3. The background false interloper

A particularly intriguing feature of NGC 7679 morphology is that the most disturbed side of the galaxy's body coincides with the position (∼29″ East) of a much fainter, slightly elongated companion one could easily misinterpret as an interacting satellite galaxy capable of distorting the outer regions of the main galaxy. The projection effect is so convincing as to induce Pogge & Eskridge (1993) to ascribe to the interaction with this object the most pronounced tidal structures of NGC 7679. The same oversight can be noticed also in the later study by Della Ceca et al. (2001).

Thanks to a long-slit spectrum obtained in run 6 with MMT we can now demonstrate that such an "intruder" is actually a background galaxy with a measured heliocentric recession velocity $V_\odot = 33\,105 \pm 5$ km s^{-1} which corresponds to $V_{3\,\mathrm{K}} = 32\,736$ km s^{-1} after applying the 3 K background correction following Fixsen et al. (1996). By adopting the proper relativistic redshift formula we derive $z = 0.1158$, i.e. approximately 7× the observed redshift of NGC 7679.

Assuming $\Omega_\mathrm{M} = 0.3$ and $\Omega_\Lambda = 0.7$ (cf. Tegmark et al. 2004), we derive an angular diameter distance of ∼400 Mpc. Since the corresponding angular scale is ∼1.94 kpc arcsec^{-1}, its observed ionized-gas rotation curve extends to $R \sim 11.6$ kpc (see Fig. 5). The mass within such a radius turns out to be ∼3×10^{10} $M_\odot$ assuming a spherical mass distribution and the galaxy seen edge-on.

3.4. The radio morphology

As pointed out above, NGC 7679 has previously been detected in a number of single-dish observations (see Duprie & Schneider 1996, and references therein). Duprie & Schneider (1996) reported that the H I line profile of the galaxy is peculiar, but cautioned against possible contamination from the neighbor Seyfert galaxy NGC 7682.

Our H I image (Fig. 6a) shows that NGC 7679 and NGC 7682 share a common gaseous envelope: an examination of the channel maps (Kuo et al., in preparation) demonstrates that this envelope comprises a tidal bridge connecting the two galaxies, as well as opposing tidal tails from the two galaxies. The extended and diffuse optical feature on the eastern side of NGC 7679 (Fig. 3a) can be identified with the inner region of this H I tidal bridge.

The total flux density of each of the three components is 54.6 ± 0.9 mJy for NGC 7679, 52.6 ± 1.0 mJy for NGC 7682, 1.1 ± 1.4 mJy for the bridge. Assuming our adopted distance of 63.9 Mpc, their radio continuum luminosities are 2.67×10^{29} erg s^{-1} Hz, 2.58×10^{29} erg s^{-1} Hz, 4.95×10^{27} erg s^{-1} Hz, respectively. The continuum emission associated with each Seyfert galaxy is not spatially resolved as seen in Fig. 6c. The latter shows an image of the continuum emission at 21 cm, most probably produced or dominated by synchrotron emission from relativistic electrons. The two strongest sources visible are those associated with NGC 7679 and NGC 7682. Interestingly, a continuum source is visible lying between NGC 7679 and 7682, and perhaps forming a bridge between these two objects. This source or bridge coincides with the H I tidal bridge connecting the two galaxies, and may be

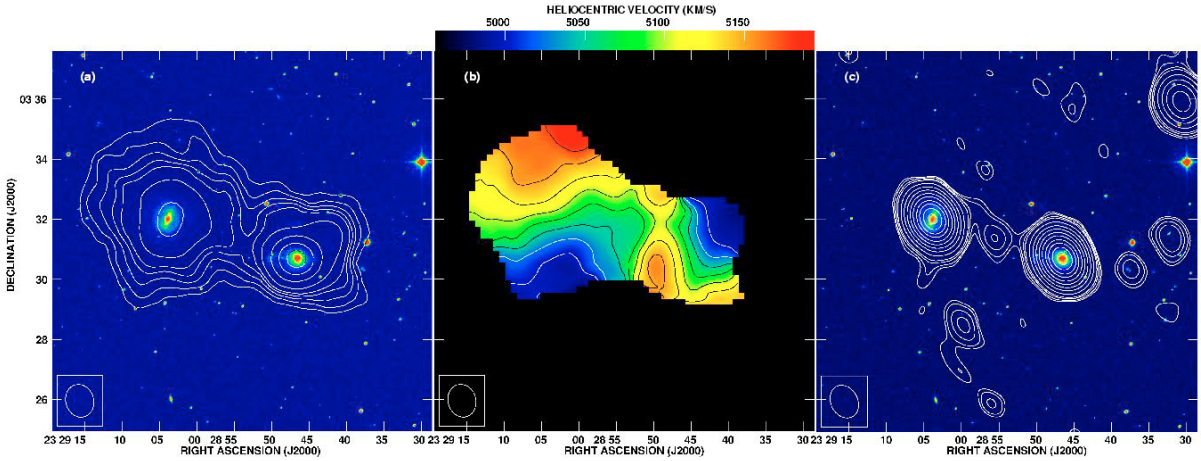

Fig. 6. a) H I total intensity (moment 0) map superposed to the optical image of NGC 7679 (*lower right*) and NGC 7682 (*upper left*). The peak flux is 2.4×10^3 Jy beam^{-1} m s^{-1}. Contour levels are (0.3, 0.9, 1.5, 2.1, 2.7, 4.5, 9, 15, 21) $\times$ 10^2 Jy beam^{-1} m s^{-1}. **b)** H I velocity field (moment 1) contour map on the total intensity (moment 0) color-coded map. Coded colors (from blue to red) are for 4750, 4775, 4800, 4825, 4850, 4875, 4900, 4925, 4950, 4975, 5000, 5025 km s^{-1}. **c)** H I continuum emission map. The peak flux is 5.3×10^{-2} Jy beam^{-1} m s^{-1}. Contour levels are (3.6, 4.8, 7.2, 9.6, 19.2, 36, 60, 96, 144, 216, 288, 384, 480) $\times10^{-4}$ Jy beam^{-1} m s^{-1}. The synthesized beam of all the maps is $68\farcs0 \times 53\farcs3$.

produced by star-formation activity in this bridge. Of course, we cannot rule out the possibility that this source is an unrelated foreground or background source.

3.5. The cold gas velocity field

Although NGC 7682 does not appear to be disturbed in the optical, not only does it exhibit extended H I tidal features, but its H I kinematic major axis shows a wide misalignment (>50°) with its optical major axis (see Fig. 6b). The highly extended tidal features indicate that this system must have started to gravitationally interact some time ago, and can be used to estimate the timescale since closest approach. More precisely, tidal features seen in both galaxies extend to about 80 kpc from each galaxy, and have a measured maximum radial velocity of ~120 km s^{-1}. If the latter also is their maximum velocity in the plane of the sky, and assuming that the gas originates from the outer regions of a disk with radius of ~20 kpc, the tidal structures would therefore have a kinematic age of ~500 Myr.

3.6. Ultraviolet energy distribution and burst dating

In Seyfert 2 galaxies the optical energy distribution toward shorter wavelengths is increasingly dominated by the so-called "featureless continuum" (FC; cf. Heckman et al. 1995). A fraction of it has to be ascribed to the reflected (polarized) light by a "hidden" Seyfert 1 nucleus (FC1) while the majority of it (FC2; appearing as a blue, unpolarized continuum) is currently thought originated in a population of hot, massive stars. Understanding the relative role of these two components is quite important for a system like NGC 7679, owing to its highly composite nature.

In order to remove the degeneracy of the above two continua observed at optical wavelengths for the youngest populations (<10 Myr; cf. Storchi-Bergmann et al. 2000), one has to move to the UV region where an ongoing starburst, when present unambiguously reveals several strong absorption stellar wind resonance lines, such as N V λ1240, Si IV λ1400 and C IV λ1550, superposed on the underlying continuum. In this respect, the continuum originated by very young stars (FC2) should not be named "featureless" at all. Besides showing the above strong stellar-wind lines, the NGC 7679 IUE spectrum (Fig. 7) reveals that C IV λ1550 does possess an outstanding P-Cygni profile (instead of being pure photospheric absorption), thus assuring that the burst we are observing is still within its early phase, dominated by strong stellar winds. Within the IUE large aperture ($10'' \times 20''$), such a burst generates an extinction-corrected Lyα flux $F_{\mathrm{Ly}\alpha}$ = 4.9×10^{-13} erg cm^{-2} s^{-1}, whose equivalent width is 37 Å.

A reliable estimate of the age of the recently formed stars (and thus an estimate of the epoch of the starburst onset in NGC 7679) can be derived by comparing its IUE/SWP spectrum with the overlapping portion of Hopkins Ultraviolet Telescope (HUT) spectra of similar starburst galaxies presented by Leitherer et al. (2002). In particular, one can easily notice the good match of NGC 7679 with both the continuum and – allowing for more pronounced P-Cygni effects – the UV absorption features of their young starburst IRAS 08339+6517 (see Fig. 7).

The match between the UV energy distributions of the two starburst objects presented in Fig. 7 is quite impressive. Both spectra have been corrected for redshift, galactic and internal extinction. The latter value has been assumed to be close to $E(B-V) \sim 0.3$ for both galaxies. In the case of IRAS 08339+6517 the absorption $A_{1500} = 2.34$ mag estimated by Leitherer et al. (2002) corresponds to $E(B-V) \sim 0.29$, if one applies the extinction curve of Savage & Mathis (1979), while for the overall line-emitting disk of NGC 7679 one can assume a value $E(B-V) \sim 0.33$ obtained by the observed ratio Lyα/H$\alpha \sim 0.9$ to be compared with the theoretical "Case B" ratio Lyα/Hβ = 31.6 for $T_{\mathrm{e}} = 10^4$ K and $\log n_{\mathrm{e}} = 4$, having assumed the standard Balmer decrement Hα/Hβ = 2.86 (see Dopita & Sutherland 2003). This strongly suggests that we are comparing young-star dominated systems very close in age. In

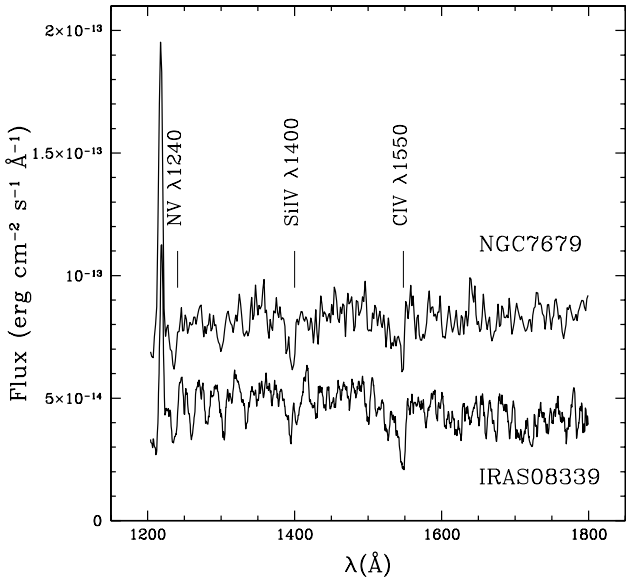

Fig. 7. Comparison of the UV spectra of NGC 7679 (IUE) and the young starburst IRAS 0339+6517 (HUT) in the region where they overlap ($\lambda\lambda$ 1200−1800 Å). Both spectra have been corrected for redshift and galactic extinction as given by Burstein & Heiles (1984). The HUT spectrum of IRAS 08339+6517 has been smoothed with a 7 pixel window. A constant amount of 4×10^{-14} flux units has been added to the NGC 7679 UV energy distribution – previously normalized to match the HUT spectrum around λ 1500 Å – for display purposes. The most prominent stellar wind absorption lines are marked.

particular, Leitherer et al. (2002) ascribe the UV spectrum of IRAS 08339+6517 to a 10 Myr-old stellar population of solar composition, though compatible with an age between 5 and 20 Myr. As a consequence, we date back to 5−20 Myr ago also the onset of star-formation episode we are witnessing today in NGC 7679. For comparison, the internal extinction we derive within the slice ($2\farcs0 \times 2\farcs4$ at PA = 0°) of the NGC 7679 covered by our own low-resoultion spectrum (run 4) by measuring its Balmer decrement, turns out to be higher ($E[B-V] \sim 0.60$). Given the tiny portion of the emitting region recorded by this latter spectrum, likely affected by local, innermost inhomogeneities, we keep $E(B-V) \sim 0.33$ as the representative absorption of the NGC 7679 disk as a whole.

3.7. The dominance of the starburst at IR wavelengths

The existence of ongoing starburst in a galaxy reflects an enhancement of the far-infrared (FIR) continuum emission, due to dust re-radiation of ultraviolet photons from hot OB stars. At the same time, in the case of a composite object like NGC 7679, one has to expect a substantial contribution to the FIR continuum by the underlying AGN. In order to identify which source dominates the IR emission in our object, one can use the classification scheme adopted by Mouri & Taniguchi (2002) on the basis of far-infrared flux densities of the IRAS database.

Having defined $F_{\rm IR}$ as the observed flux between 40 and 120 μm and $F_{\rm B}$ as the monochromatic flux at 4300 Å, respectively, the IR data of Kewley et al. (2001) imply for NGC 7679 a ratio $F_{\rm IR}/F_{\rm B} > 4$. This, in turn, implies that our object belongs to the Mouri & Taniguchi (2002) class of *starburst-dominated* Seyfert galaxies. For comparison, the nearby Seyfert 2 galaxy NGC 7682, likely interacting with NGC 7679, has to be classified within the above scheme as an *AGN-dominated* Seyfert, owing to its measured $F_{\rm IR}/F_{\rm B} < 1$ (Mouri & Taniguchi 2002). As such, the two systems, although sharing the nuclear Seyfert phenomenon, appear quite different in the mutual dominance of the central AGN and the young star emission.

3.8. Star formation rate

Correcting for the galactic extinction by Burstein & Heiles (1984), our pure emission-line image of NGC 7679 gives a extinction corrected total flux $F_{\rm H\alpha+[NII]} = 8.0{\times}10^{-13}$ erg cm^{-2} s^{-1}. The innermost ($r \leq 3''$) region ($r \leq 3''$) – i.e. the central spiral pattern – gives a corresponding flux $F_{\rm H\alpha+[NII]} = 5.9 \times 10^{-13}$ erg cm^{-2} s^{-1}. As such, the latter region alone provides approximately 75% of the total Hα+[N II] emitted flux. The spectrophotometry of Contini et al. (1998), showing that the fraction of light due to Hα amounts to 64% of the total Hα+[N II] emission, allows us to approximately correct such flux for the contamination of the [N II] $\lambda\lambda$6548, 6583 doublet emission, thus giving a "pure" Hα flux received from NGC 7679 of 5.1×10^{-13} erg cm^{-2} s^{-1}. Moreover, one has to assume that the latter value is still affected by some amount of internal extinction, which, in localized regions of starburst galaxies, can be as high as A(Hα) ~ 2 mag (cf. Kennicutt 1998). In the specific case of NGC 7679, assuming $E(B-V) = 0.33$ as the color excess due to its internal extinction close to the center (see Sect. 3.6), the intrinsic Hα flux is 1.1×10^{-12} erg cm^{-2} s^{-1}. The latter value, properly transformed into the corresponding $L_{\rm H\alpha}$, allows us, in turn, to estimate the current star formation rate.

On the basis of our adopted distance of 63.9 Mpc, the above flux translates into an Hα luminosity of 5.4×10^{41} erg s^{-1}. By assuming the calibration of Kennicutt et al. (1994) this implies a $SFR \sim 4\ M_\odot$ yr^{-1}. An independent SFR estimate can be derived also by the UV continuum measured in the IUE spectrum. After correcting for redshift, and galactic extinction, the measured average flux in the absorption-free wavelength range between 1425 and 1515 Å is $F_\lambda = 2.6 \times 10^{-13}$ erg cm^{-2} s^{-1} Å^{-1}. This translates into a luminosity of 9.6×10^{28} erg s^{-1} Hz^{-1} corresponding, with the calibration given by Kennicutt (1998), to a $SFR \sim 13\ M_\odot$ yr^{-1}. The two levels of star formation (i.e. the one derived from the optical recombination line and that obtained from the UV continuum) are then quite similar and appear relatively high, being comparable to that shown by other similarly disturbed starburst systems like, for instance NGC 7673 ($SFR \sim 10$−$20\ M_\odot$ yr^{-1}; Homeier et al. 2002).

For the radio data, using the empirical correlation between the radio continuum luminosity at 1.4 GHz and SFR (Condon 1992; Lou & Bian 2005) we find a $SFR \sim 7\ M_\odot$ yr^{-1} for NGC 7679, 6 $M_\odot$ yr^{-1} for NGC 7682, and 0.1 $M_\odot$ yr^{-1} for the bridge region. For both NGC 7679 and NGC 7682, the computed SFR are, of course, upper limits as a part of the radio emission could arise from the central AGN. For NGC 7679

such an estimate is within the range derived from optical and UV measurements.

3.9. The close encounter with NGC 7682

Having definitely excluded any role of the close background companion in the origin of distorted morphology of NGC 7679, the most likely culprit becomes NGC 7682, the face-on barred spiral located only ∼4′.5 North-East. This latter galaxy – itself a Seyfert 2 system with an almost identical redshift – offers straightforward evidence, thanks to the radio observations discussed above, of a tidal interaction that happened a few hundred million years ago. Although interaction is often invoked as a starburst-triggering phenomenon (cf. Greene et al. 2004), whether this specific encounter played a role in the onset of the current central starburst in NGC 7679 remains difficult to say, because of the evident youth of the latter phenomenon.

4. NGC 7679 in the framework of the AGN-starburst connection issue

NGC 7679, showing simultaneously a vigorous starburst in the optical and a powerful AGN in the X-ray waveband, is a prototypical composite object.

We derived extinction-corrected diagnostic ratios from optical emission lines, namely $\log([\mathrm{O\ III}]\,\lambda5007/\mathrm{H}\beta) = 0.172$ and $\log([\mathrm{N\ II}]\,\lambda6583/\mathrm{H}\alpha) = -0.343$. Such observed ratios are consistent with the earlier corresponding values measured by Dahari (1985). On the basis of the most recent diagnostic diagrams by Kauffmann et al. (2003) and its low [O III] λ5007 luminosity ($L_{[\mathrm{OIII}]} = 3.2 \times 10^6\ L_\odot$) i.e. the main parameter they adopt as an AGN activity tracer, NGC 7679 falls closer to the region of proper starburst galaxies (Fig. 8) also in agreement with previous results by Panessa & Bassani (2002).

Given the dominance of star formation at optical wavelengths for composite systems, specific indicators capable of tracing "pure" AGN power by disentangling it from superposed vigorous star formation are required. Two useful indicators are currently known, namely the absorption-corrected intrinsic 2−10 keV X-ray luminosity and the luminosity of broad hydrogen emission lines which come from the high-velocity gas around the central supermassive black hole in the AGN. A recent study of the correlation between these two quantities (for type-1 AGNs) is given by Imanishi & Terashima (2004). Although the quality of our own optical spectra of NGC 7679 are not suitable to study in detail its faint broad Balmer component, we resorted – for its classification – to the high S/N spectrum of Kewley et al. (2001), who identified a broad component with $FWHM \sim 2000$ km s^{-1} at the basis of its narrow Hα. From Della Ceca et al. (2001) we know that the luminosity of such a broad component is estimated by the above authors to be $L_{\mathrm{broad\ H}\alpha} = 8.0 \times 10^{40}$ erg s^{-1}. Assuming the 2−10 keV X-ray luminosity by Della Ceca et al. (2001) scaled to our adopted distance ($L_X = 6.1 \times 10^{42}$ erg s^{-1}) NGC 7679 falls among the dust-unabsorbed Type 1 AGNs with an underluminous broad Hα component, as shown in Fig. 9. This is in strict agreement with the proposed classification by Della Ceca et al. (2001).

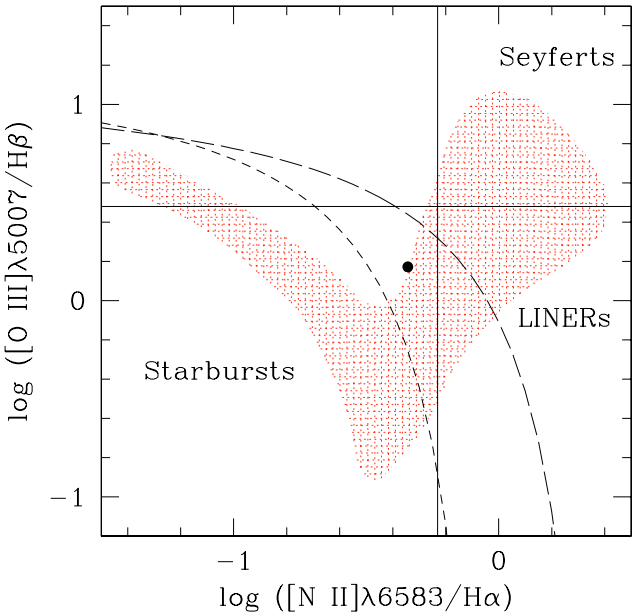

Fig. 8. The location of NGC 7679 in the optical emission-line diagnostic diagram of Kauffmann et al. (2003; filled circle). The short and long dashed lines mark the demarcation between starburst galaxies and AGNs according to Kauffmann et al. (2003) and Kewley et al. (2001), respectively. The vast majority of the galaxies studied by Kauffmann et al. (2003) are located in the hatched region.

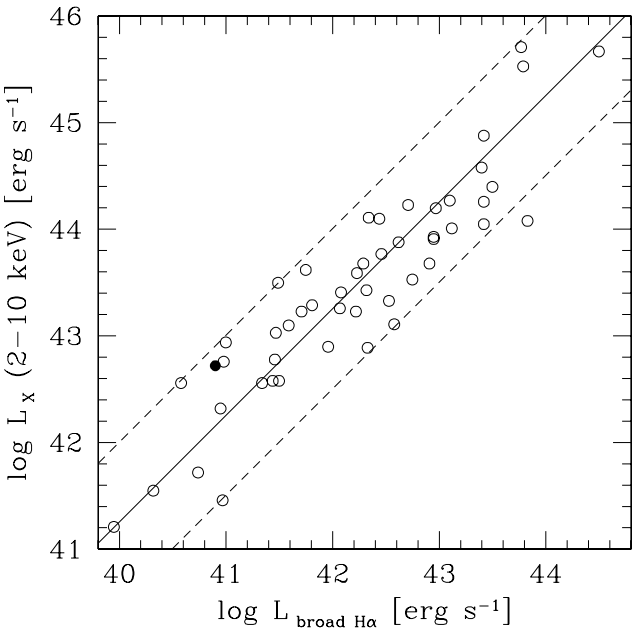

Fig. 9. The location of NGC 7679 in the X-ray/optical diagnostic diagram of Imanishi & Terashima (2004; filled circle). Luminosities of NGC 7679 are taken from Della Ceca et al. (2001). The region of dust-unabsorbed Type 1 AGNs (open circles) is marked with dashed lines.

At the same time NGC 7679 offers much more to the researchers currently exploring the elusive link between AGN activity and ongoing SB. For instance, hosting simultaneously a bar and having undergone a past interaction, it has at least two distinct efficient mechanisms to drive gas from its outer parts

to the nuclear region (cf. Gonzàlez Delgado et al. 1998). Once the expected inward flow of gas reaches its central region, it is capable not only of triggering star formation, but also of forming a gas reservoir (in the form of a molecular torus) which likely feeds the nucleus itself. This twofold scenario is further enriched by the presence of an amount of molecular hydrogen – as derived from radio CO observations (Kandalyan 2003) – comparable to that of neutral hydrogen (a few 10^9 $M_\odot$). What is more, unlike other Markarian galaxies, the CO in NGC 7679 distinguishes itself for having its line *FWHM* larger than that of its H I line. Since the CO gas kinematics reveals the rotation and/or velocity dispersion close to the nucleus, this phenomenon is interpreted as due to a rapidly rotating nuclear disk (cf. Kandalyan 2003). As such, part of this circumnuclear gas is likely prone to streaming inward with velocities $\sim$100 km s^{-1} directly onto the nucleus (cf. Regan et al. 1999), so that a phenomenon usually unobservable in other AGN, appears at the center of this galaxy.

5. Summary and conclusions

NGC 7679 has a wealth of distinct interlaced phenomena. The investigation of its special properties is made easier both by its relative proximity and projected orientation.

Among the most interesting features we were able to identify are the following:

1. High resolution Hα imaging shows several knots and loose ionized gas debris. In addition it reveals a central circumnuclear star-forming spiral/ring capable of producing $\sim$75% of the optical line emission within a radius of $\sim$1 kpc. Observations from the literature suggest that this central region contains a large amount of molecular gas, likely giving rise to a stream moving inward, so as to possibly fuel the galaxy nucleus.
2. An ionized gas ring-like feature is part of the centrally located starburst dominating the galaxy emission both at optical and IR wavelengths. Such an event is characterized by an *SFR* of $\sim$10 $M_\odot$ yr^{-1}, as derived from optical and UV observations, and consistent also with 14 GHz radio continuum observations. The onset of the phenomenon is not earlier than 20 Myr ago, as shown by the prominent stellar wind absorption lines seen in its IUE ultraviolet spectrum shortward of 2000 Å.
3. The ionized gas velocity field can be traced out to $r \sim 20''$ (corresponding to 5–6 kpc). Although the latter appears characterized by a basically regular rotation within the innermost (15″) region, clear signs of asymmetries (i.e, perturbations) are recognizable at a radius just beyond such a distance.
4. The overall neutral gas velocity field (as derived from H I radio observations) is perhaps more indicative of the past history of the binary system. In particular, although reflecting the combined outer kinematics of both NGC 7679 and NGC 7682, it still allows observers to isolate individual kinematic properties. In this respect, the most outstanding outcome is the macroscopic misalignment of the H I and optical kinematic major axes of the companion galaxy NGC 7682 (ΔPA > 50°).
5. The extent of the neutral gas common envelope, in turn, suggests that a close encounter likely happened a few hundred million years ago. Its relationship with the current, much more recent central starburst has to be further investigated.
6. We unambiguously established that the angularly close fainter companion galaxy of NGC 7679, superposed by chance on its highly disturbed eastern arm, is indeed an object located much farther away, in the deep background of the main galaxy and, as such, is certainly not involved in its dynamical evolution.
7. Della Ceca et al. (2001) are induced look at NGC 7679 as a highly peculiar object owing to its selective absorption apparently not affecting its X-ray AGN emission, so as to ascribe to its nucleus "unique" physics/geometry. Conversely, the present analysis leads to a less extreme classification of NGC 7679 i.e. as a "normal" low-luminosity Seyfert 1 object (given the ratio of its broad Hα luminosity vs. hard X luminosity, cf. Fig. 9) and a transition object at optical wavelengths (cf. Fig. 8. This allows us to conclude that NGC 7679 is a galaxy where starburst and a mildly obscured AGN (given the upper limit of the column density of the neutral hydrogen corresponding to $E(B-V) \sim 0.1$ according to the above authors) coexist with the starburst dominating the bolometric luminosity.

Acknowledgements. M.C. acknowledges support from a VENI grant 639.041.203 awarded by the Netherlands Organization for Scientific Research (NWO).

References

Arp, H. 1966, ApJS, 14, 1
Burstein, D., & Heiles, C. 1984, ApJS, 54, 33
Condon, J. J. 1992, ARA&A, 30, 575
Contini, T., Considère, S., & Davoust, E. 1998, A&AS, 130, 285
Corsini, E. M., Pizzella, A., Sarzi, M., et al. 1999, A&A, 342, 671
Dahari, O. 1985, ApJS, 57, 643
de Vaucouleurs, G., de Vaucouleurs, A., Corwin, H. G., et al. 1991, Third Reference Catalogue of Bright Galaxies (Dordrecht: Springer-Verlag)
Della Ceca, R., Pellegrini, S., Bassani, L., et al. 2001, A&A, 375, 781
Dopita, M. A., & Sutherland, R. S. 2003, Astrophysics of the Diffuse Universe (Dordrecht: Springer-Verlag)
Duprie, K., & Schneider, S. E. 1996, AJ, 112, 937
Durret, F., & Warin, F. 1990, A&A, 238, 15
Elvis, M., Schreier, E. J., Tonry, J., Davis, M., & Huchra, J. P. 1981, ApJ, 246, 20
Fiore, F., La Franca, F., Vignali, C., et al. 2000, NewA, 5, 143
Fixsen, D. J., Cheng, E. S., Gales, J. M., et al. 1996, AJ, 473, 576
González Delgado, R. M., Heckman, T., Leitherer, C., et al. 1998, ApJ, 505, 174
Greene, J., Lim, J., & Ho, P. T. P. 2004, ApJS, 153, 93
Gu, Q. S., Huang, J. H., de Diego, J. A., et al. 2001, A&A, 374, 932
Heckman, T., Krolik, J., Meurer, G., et al. 1995, ApJ, 452, 549
Homeier, N. L., Gallagher, J. S., III, & Pasquali, A. 2002, A&A, 391, 857

Imanishi, M., & Terashima, Y. 2004, AJ, 127, 758
Jogee, S., Knapen, J. H., Laine, S., et al. 2002, ApJ, 570, L55
Kandalyan, R. A. 2003, A&A, 398, 493
Kauffmann, G., Heckman, T. M., Tremonti, C., et al. 2003, MNRAS, 346, 1055
Kennicutt, R. C., Tamblyn, P., & Congdon, C. W. 1994, ApJ, 435, 22
Kennicutt, R. C. 1998, ARA&A, 36, 189
Kewley, L. J., Heisler, C. A., Dopita, M. A., & Lumsden, S. 2001, ApJS, 132, 37
Krajnović, D., Cappellari, M., de Zeeuw, P. T., & Copin, Y. 2005, MNRAS, in press
Leitherer, C., Li, I.-H., Calzetti, D., & Heckman, T. 2002, ApJS, 140, 303
Lou, Y.-Q., & Bian, F.-Y. 2005, MNRAS, 358, 1231
Matt, G. 2001, MSAIt, 72, 51
Mouri, H., & Taniguchi, Y. 2002, ApJ, 565, 786
Panessa, F., & Bassani, L. 2002, A&A, 394, 435
Pogge, R. W., & Eskridge, P. B. 1993, AJ, 106, 1405
Regan, M. W., Sheth, K., & Vogel, S. N. 1999, ApJ, 526, 97
Savage, B. D., & Mathis, J. S. 1979, ARA&A, 17, 73
Sparks, W. B., Ford, H. C., & Kinney, A. L. 1993, ApJ, 413, 531
Storchi-Bergmann, T., Raimann, D., Bica, E. L. D., & Fraquelli, H. A. 2000, ApJ, 544, 747
Tegmark, M., Strauss, M. A., Blanton, M. R., et al. 2004, PhRvD, 69, 103501
Veilleux, S., Kim, D.-C., Sanders, D. B., Mazzarella, J. M., & Soifer, B. T. 1995, ApJS, 98, 171
Véron-Cetty, M. P., & Véron, P. 2001, A&A, 374, 92